

Exciton line shapes of GaAs/AlAs multiple quantum wells

J. Humlíček, E. Schmidt, L. Bočánek, and R. Švehla

Department of Solid State Physics, Faculty of Science, Masaryk University, Kotlářská 2, 611 37 Brno, Czech Republic

K. Ploog

Max-Planck-Institut für Festkörperforschung, Heisenbergstrasse 1, D-7000 Stuttgart, Germany

(Received 27 April 1992; revised manuscript received 13 November 1992)

We present a detailed study of the photoluminescence (PL) spectra of GaAs/AlAs multiple-quantum-well structures with well thicknesses of 83.8 and 78.1 Å in the temperature range from 16 to 320 K. We examine the relation of luminescence and absorption, find a part of the heavy-hole exciton line suitable for a detailed comparison with model profiles, and perform a line-shape analysis using Lorentz-Gauss profiles expressed efficiently in terms of the complex probability function. We have observed the Stokes shift (about 4 meV at 16 K, which vanishes fast with increasing temperature) of the PL peak with respect to the center of the exciton absorption, and explain it quantitatively assuming a detailed thermodynamical balance of excitons and radiation. The inhomogeneous broadening of the line is Gaussian and the increase of the homogeneous Lorentzian component is found to be nearly linear in the 50–320-K region.

I. INTRODUCTION

Excitonic effects at the fundamental absorption gap of multiple-quantum-well (MQW) structures have been studied extensively aiming at both fundamental and technologically important properties (see, e.g., several comprehensive reviews^{1,2} and references therein). The photoluminescence (PL) technique proved to be a valuable tool to study the nature of the lowest excitations; the first, and up to now the best understood, structures consist of GaAs quantum wells (QW's) with $\text{Al}_x\text{Ga}_{1-x}\text{As}$ barriers.^{3,4} In particular, the interaction of excitons with phonons has been investigated many times by various optical methods, as reviewed recently.^{5,6} A recent study of exciton-phonon coupling in the GaAs/ $\text{Ga}_x\text{Al}_{1-x}\text{As}$ system has used the technique of normal-incidence reflectance.⁷

In this paper we present results of a comprehensive study of the PL spectra of two well-characterized GaAs/AlAs MQW structures. Our aim was to obtain reliable, low-noise PL signals in a wide temperature range, enabling us to perform a detailed line-shape analysis. In order to elucidate the behavior of the PL spectra at the lowest temperatures, we compare them with normal-incidence reflectance spectra. The low-noise reflectance spectra allow multiple numerical differentiation, which suppresses the role of inevitable interference effects within MQW films.⁸

The paper is organized as follows. In Sec. II we describe the experiments. The assumptions used in the line-shape analysis are addressed in Sec. III, where a link of emission and absorption profiles for the assumed equilibrium is given first (Sec. III A); we choose a notation suitable for discussing the possible influence of self-absorption and dispersion of the refractive index in the PL spectra. Section III B is devoted to a description of line profiles resulting from independent Lorentz and

Gauss broadening that proved to be an excellent choice for our spectra. We present a convenient form of the absorption lines and the corresponding dispersion profiles, using an easy-to-evaluate special function. Section IV summarizes the results of the line-shape analysis, and the final discussion of the temperature evolution is given in Sec. V.

II. EXPERIMENT

The two GaAs/AlAs MQW samples of the present study were grown by molecular-beam epitaxy (MBE) on (100) semi-insulating GaAs substrates. They were characterized by multiple-angle-of-incidence ellipsometry and by interference patterns in normal-incidence reflectance.⁹ From the total MQW film thicknesses, 762 ± 3 and 847 ± 4 nm, we obtain the mean thicknesses of a single QW in the structure of 78.1 ± 0.5 Å in one sample and 83.8 ± 0.5 Å in the other sample, respectively. The latter results differ slightly from the target value of 84.9 Å (i.e., 30 monolayers) that has been used to control the MBE growth via the intensity oscillations of reflection high-energy electron diffraction.

The PL spectra were measured with a 1-mW HeNe pump laser, with all wavelengths except the red 633-nm (1.96-eV) line filtered off. The samples were mounted in a closed-cycle cryostat operating in the 16–320 K range. The increase of the sample temperature due to the pumping beam was negligible at this low power level. The signal was analyzed by a 0.6-m grating monochromator and detected with a GaAs photomultiplier. The spectral resolution was kept high enough to prevent instrumental broadening, but was adjusted to the increasing spectral width and decreasing strength of the PL signal with increasing temperature. Namely, we have measured with wider slits at higher temperatures, in order to reduce the noise in the broader and weaker spectra. A computer-

driven amplification system was used to accumulate several tens samples of the signal at each spectral point. One spectral run took typically about 20 min, with temperature fluctuations less than 1 K. We have reached a noise level of $\sim 5 \times 10^{-4}$ of the peak PL intensity at the lowest temperature (i.e., for the strongest signal). At room temperature and slightly above (320 K), the noise did not exceed about 1% of the peak signal, which is still acceptable for our purpose. Special care was taken in obtaining reliable base lines for the spectra that are of primary importance for the weak signals. The dark current of the detector and zero level of the amplifying system did not drift above the noise level.

The normal-incidence reflectance was measured with the same setup. A stable 150-W tungsten lamp was used to produce monochromatic light. The ratio of signals after reflection on the sample and a single-crystal silicon slice was multiplied by the known reflectivity of silicon.⁸ Pronounced structures due to the heavy- and light-hole excitons appear in all reflectance spectra up to highest temperature. However, strong interference patterns are observed below the excitonic edge that influence the excitonic line shapes.¹⁰ Here we use reflectance as a probe enabling us to obtain primarily the spectral position of the excitonic absorption. This is fairly straightforward by using the numerical differentiations and the symmetry of the derivative spectra.^{8,10} It would be possible to analyze the line profiles in the reflectance spectra, but the multiple reflection within the MQW film would have to be considered. We have therefore chosen the PL spectra for the consequent line-shape analysis.

III. SPECTRAL LINE SHAPES

A. Emission and absorption profiles

We assume that the principle of the detailed balance¹¹ applies for the whole temperature range and for the pump powers used here. Then, the emitted intensity of photons with energy E is proportional to the probability of absorption, multiplied by the density of photons at the same energy,¹¹

$$I_e = \text{const} \times \frac{\alpha}{n} \frac{E^2 n^3}{\exp(E/kT) - 1}. \quad (1)$$

Here, α is the absorption coefficient, n is the real part of the complex refractive index $N = n(1 + i\kappa)$, κ is the Boltzmann constant, and T is the temperature. The excited states that do not contribute to the luminescent intensity I_c decay nonradiatively. The balance at each photon energy in the spectrum governs the distribution of probabilities into the radiative and nonradiative energy-loss processes. The most probable channels for nonradiative decay are multiphoton processes; although decisive for luminescent power, these processes are not expected to produce any significant spectral dependence of the emitted light in the narrow range of exciton lines. The optical parameters α and n are related to the complex dielectric function $\epsilon = \epsilon_1 + i\epsilon_2$,

$$n(1 + i\kappa) = \sqrt{\epsilon_1 + i\epsilon_2}, \quad \alpha = 4\pi\nu n\kappa, \quad (2)$$

where ν is the wave number corresponding to the photon energy E (ν in cm^{-1} is equal to $8065E$ for E in eV). Since $E \gg kT$ in our spectral region, Eq. (1) reduces to

$$I_e \sim n\epsilon_2 E^3 \exp(-E/kT). \quad (3)$$

The observed PL intensity is influenced by the penetration depth of the exciting light, and by the absorption and reflection of the generated photons in the MQW film. Neglecting the multiple reflections of the pump beam and assuming quantum yield independent of intensity, the rate of generation is proportional to α_x , and decays as $\exp(-\alpha_x D)$ with the depth D below the sample surface; here, α_x is the absorption coefficient at the exciting photon energy E_x . The photon emitted in the depth D can be absorbed with the probability proportional to $\exp(-\alpha D)$ and reflected at the sample surface with the probability of $R = |N - 1|^2 / |N + 1|^2$. The contributions from all depths can be easily summed assuming a semi-infinite medium. The registered PL intensity is

$$I \sim I_e (1 - R) \alpha_x \int_0^\infty \exp[-(\alpha_x + \alpha)D] dD = \frac{I_e \alpha_x (1 - R)}{\alpha_x + \alpha}. \quad (4)$$

Equations (3) and (4) can be combined in the following convenient form:

$$I_c = I E^{-3} \exp(E/kT) \sim \epsilon_2 \frac{\alpha_x n}{\alpha_x + \alpha} (1 - R). \quad (5)$$

For an absorption band that is not too strong to produce a pronounced dispersion of the refractive index n , the spectral shape of I_c is essentially determined by the absorptive part ϵ_2 of the dielectric function. Since our goal is to compare the luminescence spectra with the absorption profiles described by the Gauss-Lorentz line shapes in Sec. III B we point out the relation of I_c to the imaginary part ϵ_2 of the dielectric function. If the penetration depth $1/\alpha_x$ of the exciting light was not negligible against $1/\alpha$, the self-absorption would tend to flatten the luminescence structure in I_c compared with the absorption band ϵ_2 due to the factor $1/(\alpha_x + \alpha)$. In any case, the modified PL profile I_c is strongly influenced by the Boltzmann factor $\exp(E/kT)$, especially at low temperatures. Let us note that the integration over the semi-infinite medium in Eq. (4) removes the dependence of luminescent intensity on the absorption coefficient α_x at the pumping energy for $\alpha \ll \alpha_x$, i.e., for $\alpha_x / (\alpha_x + \alpha) \approx 1$. This condition is typically fulfilled in the photoluminescence excitation (PLE) experiments.³ Thus, the necessary condition for observing the PLE signal related to α_x is the possibility of a fraction of the pumping light being absorbed in the substrate, after passing the studied layer.

A comparison of the measured PL intensity I and the corresponding I_c spectra is shown in Fig. 1. Due to the low value of the thermal energy, $kT \approx 1.38$ meV at $T = 16$ K, the peak of the 16-K spectrum is shifted strongly towards higher energies. The high-energy side of the I_c peak is very noisy because it is a product of the measured low PL signals I with the large values of the Boltzmann

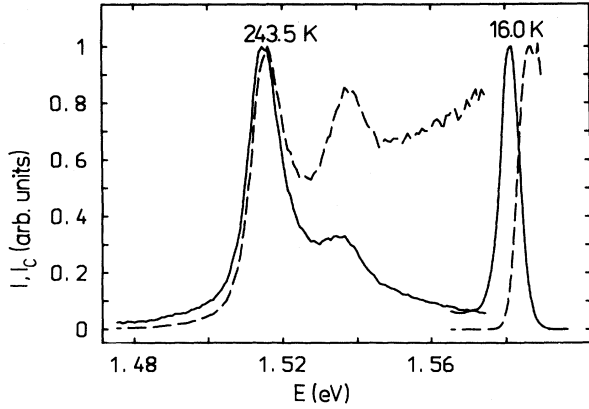


FIG. 1. Measured PL signals I (solid lines) and corrected spectra I_c of Eq. (5) (dashed lines) at two temperatures, for the 83.8-Å MQW sample. All spectra are normalized to the unit peak height.

factor $\exp(E/kT)$. In addition, any spurious background signal at the high-energy wing (which is always non-negative because of the analog-digital conversion of our amplification system) tends to produce a spurious exponential rise of the I_c spectrum. This inevitable instability is the reason for cutting the displayed range of our I_c spectra in the high-energy range of “zero” luminescent signal I . Because of the low density of the high-energy photons at thermal equilibrium, the light-hole exciton band appears in PL only at higher temperatures and is still suppressed compared with the absorption spectra.

B. Lorentz-Gauss line shapes

The complex dielectric function of a damped oscillator has the Lorentzian line shape

$$\varepsilon_L(E) = \varepsilon_\infty + \frac{F}{E_0^2 - E^2 - iE\Gamma_L}, \quad (6)$$

where E , F , E_0 , and Γ_L are the photon energy, oscillator strength, resonant energy, and damping parameter, respectively. The real constant ε_∞ is included to account for contributions to the polarizability arising from the absorption at higher photon energies. For $\Gamma_L \ll E_0$, the function of Eq. (6) can be approximated by

$$\varepsilon_L(E) = \varepsilon_\infty + \frac{F}{E_0} \left[\frac{1}{2(E + E_0) + i\Gamma_L} - \frac{1}{2(E - E_0) + i\Gamma_L} \right]; \quad (7)$$

the imaginary part of the second term in square brackets has a peak at $E = E_0$, with the full width at half maximum (FWHM) equal to Γ_L .

Let us assume that the resonant energy E_0 fluctuates randomly with the Gaussian probability density

$$f_G(E_0) = \frac{1}{\sqrt{2\pi}\Gamma_G} e^{-[(E_0 - \langle E_0 \rangle)^2]/2\Gamma_G^2}, \quad (8)$$

where $\langle E_0 \rangle$ is its mean value and Γ_G is the standard deviation. These random fluctuations modify the Lorentzian line shapes. The resulting Lorentz-Gauss (LG) profiles are obtained by summing ε_L with the corresponding Gaussian weights, i.e., by the convolution

$$\begin{aligned} \varepsilon_{LG}(E) &= \int_{-\infty}^{\infty} \varepsilon_L(E) f_G(E_0) dE_0 \\ &= \varepsilon_\infty + \frac{F}{\sqrt{2\pi}\Gamma_G} \int_{-\infty}^{\infty} \frac{e^{-[(E_0 - \langle E_0 \rangle)^2]/2\Gamma_G^2}}{E_0^2 - E^2 - iE\Gamma_L} dE_0. \end{aligned} \quad (9)$$

Using the approximate form of Eq. (7) we obtain, after a fairly straightforward calculation, the following convenient form of the LG profiles:

$$\begin{aligned} \varepsilon_{LG}(E) \approx \varepsilon_\infty + \frac{\sqrt{\pi}F}{2E_0\Gamma_G} i \left[w \left[\frac{E - \langle E_0 \rangle}{\Gamma_G} + i \frac{\Gamma_L}{2\Gamma_G} \right] \right. \\ \left. - w \left[\frac{E + \langle E_0 \rangle}{\Gamma_G} + i \frac{\Gamma_L}{2\Gamma_G} \right] \right]. \end{aligned} \quad (10)$$

Here,

$$w(z) = \frac{i}{\pi} \int_{-\infty}^{\infty} \frac{e^{-t^2}}{z - t} dt, \quad y > 0 \quad (11)$$

is the *complex probability function* of the complex argument $z = x + iy$ that has been extensively tabulated.¹² Its real and imaginary parts obey the Kramers-Kronig relations on the straight lines $y = \text{const}$.¹³

The function w can be evaluated very efficiently using rational approximants.¹³ Its asymptotic behavior

$$w(z) \rightarrow i/(\sqrt{\pi}z) \quad \text{for } |z| \rightarrow \infty \quad (12)$$

results directly from the differential equation $w'(z) + 2zw(z) = 2i/\sqrt{\pi}$, $w(0) = 1$.¹² Consequently, the LG profiles of Eq. (10) converge to the Lorentzians of Eq. (7) for $|E - \langle E_0 \rangle| \gg \Gamma_G$. In other words, the wings of

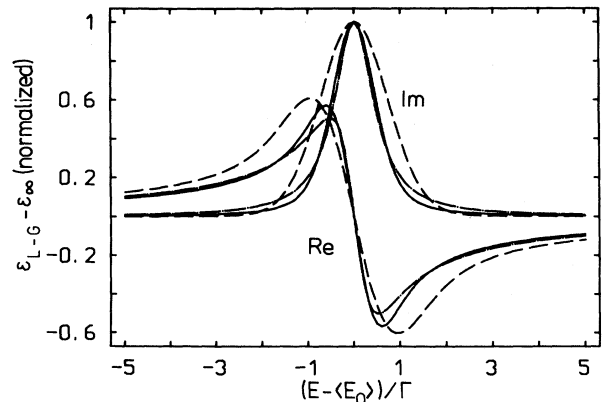


FIG. 2. Real (Re) and Imaginary (Im) parts of the Lorentz-Gauss profiles with $(\Gamma_L/\Gamma, \Gamma_G/\Gamma)$ equal to (1,1) (solid lines), (0,1,1) (dashed lines), and (1,0,1) (dashed-dotted lines).

the LG profiles are Lorentzian, whenever $\Gamma_L > 0$. For a negligible Lorentzian width $\Gamma_L \rightarrow 0$, we can still use Eq. (10) to find the spectral form of the Gaussian profile. Since $\text{Re}\{w(x)\} = \exp(-x^2)$ for real x , the imaginary part of Eq. (10) is proportional to

$$\exp\left[\frac{(E - \langle E_0 \rangle)^2}{\Gamma_G^2}\right] - \exp\left[\frac{(E + \langle E_0 \rangle)^2}{\Gamma_G^2}\right].$$

Consequently, the FWHM of the Gaussian peaks centered at $\pm \langle E_0 \rangle$ is $2\sqrt{\ln(2)}\Gamma_G \approx 1.665\Gamma_G$ for $\Gamma_G \ll |\langle E_0 \rangle|$.

Representative LG profiles are plotted in Fig. 2, including their real parts; all energies are given in arbitrary units of Γ , $\Gamma \ll |\langle E_0 \rangle|$. The profiles were normalized to the unit height of their imaginary parts. The spectral shapes with different Lorentzian and Gaussian contributions to their widths are distinct. Their broadening parameters Γ_L and Γ_G can be obtained together with the strength F and central energy $\langle E_0 \rangle$ by fitting the line shapes in a sufficiently wide spectral range.

IV. RESULTS

The measured PL spectrum at 16 K and the corresponding I_c profile of Eq. (5) are shown in Fig. 3. The latter is shifted by about 4 meV towards higher energies, which is comparable to the width of the structure [the FWHM of the asymmetric $I(E)$ band is 6.0 meV]. The peaks are due to the lowest excitation state formed from the confined heavy-hole (hh) end electron (e) states. In order to compare the spectral positions with the energy of the exciton absorption, the normal-incidence reflectance R and the d^2R/dE^2 spectra are plotted in Fig. 3. The differentiated reflectance displays clearly the hh- e and lh- e (lh denotes light hole) bands centered at 1.586 and 1.607 eV, respectively. The spectral shape of the reflectance depends in a complex way on the multiple reflections within the MQW film. However, the symmetry property of the differentiated or modulated spectra

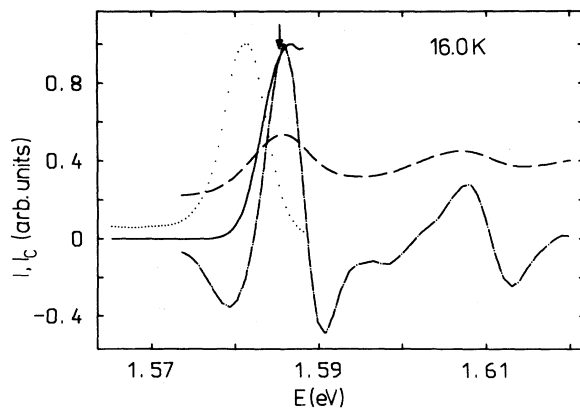


FIG. 3. Measured PL signals I (dots), I_c (corrected for the photon statistics, solid line), reflectance (dashed line), and negative second derivative of reflectance (dashed-dotted line), for the 83.8-Å MQW sample at 16 K. All spectra were arbitrarily scaled. The arrow shows the hh exciton energy obtained by fitting the low-energy wing of I_c with the Lorentz-Gauss profile.

can be used to find reliable values of the transition energies.¹⁰ The hh- e energy of 1.5853 ± 0.0004 eV obtained from the I_c spectrum by the fitting procedure described below is in very good agreement with the above value derived from the twice differentiated reflectance.

The low-energy wing of the corrected PL signal I_c is shown in detail in Fig. 4. We expect that it is dominated by the contribution of the ground state of the exciton, since the excited states, and the onset of two-dimensional continuum absorption, lie several meV above the ground state.¹ We therefore expect a good agreement between the symmetric ε_2 line shape of a single excitonic transition and the low-energy tail of I_c . We show in Fig. 4 the best-fit LG profile in the range up to $\sim \frac{3}{4}$ of the unit peak height; the mean-square deviation from the measured I_c is 5×10^{-4} which is the noise level. If we try to fit the I_c profile in the range of its maximum and above, clear systematic discrepancies appear, as shown in Fig. 4. On the other hand, by using a too low cutoff energy, the fitting becomes less sensitive to the parameters [the position $\langle E_0 \rangle$, the broadening energies Γ_L and Γ_G , and the strength F of Eq. (10)]. The evolution of the first three of these parameters with the upper limit of the fitted range is shown in Fig. 5. The systematic differences decrease with decreasing E_{\max} and reach the noise level slightly below the peak position. At the same time the broadening parameters and the exciton energy saturate at constant values. This is typical of all the PL spectra studied here. We have therefore chosen the fitting range extending to the energy below the peak, where the I_c signal reaches 70–80% of its maximum value. With this choice all the spectra were fit by the LG profiles within the random noise.

The behavior of Fig. 5 can be easily explained. The LG excitonic peak overlaps on the high-energy side with the contribution of excited states, with the two-dimensional continuum, and with the ground state of the lh exciton. The last contribution is weaker and a substantial overlap occurs at higher temperatures only. The increase of the I_c signal at the high-energy tail pushes the

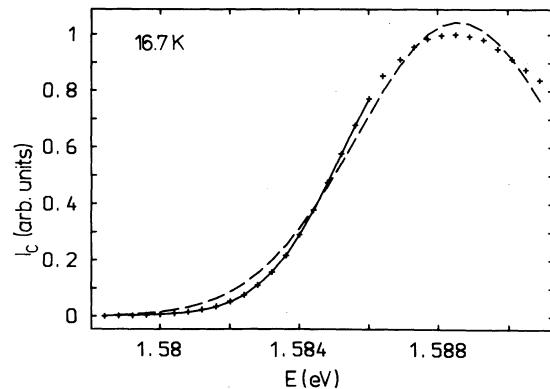


FIG. 4. Measured I_c spectrum for the 78.1-Å MQW at 16.7 K (crosses). The best-fit LG profiles in the region below $E_{\max} = 1.586$ eV is indicated by the solid line, and in the whole displayed range by the dashed line.

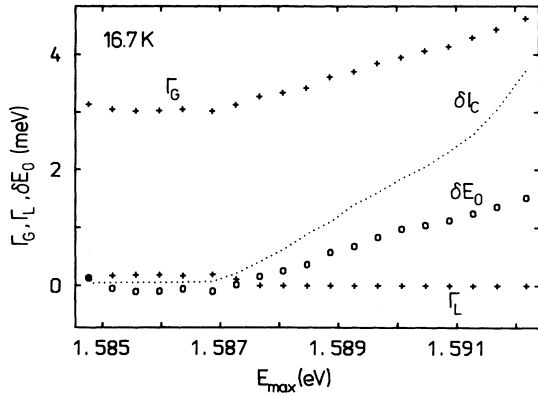


FIG. 5. Best-fit parameters vs cutoff energy for the line shape of Fig. 4; δE_0 is the shift of E_0 from an arbitrarily chosen value. The mean-square deviation δI_c from the best-fit spectra in percent of the peak height is shown by the dotted line.

position of the best-fit line upwards. It also makes the decrease in the low-energy tail steeper, which increases the Gaussian width Γ_G and decreases Γ_L , as seen in Fig. 5. A decomposition of the spectrum measured above room temperature into the lowest LG profile and the higher-lying contributions is shown in Fig. 6. The solid line is centered at $E_0 = 1.480$ eV and the broadening parameters are $\Gamma_G = 3.2$ meV and $\Gamma_L = 7.5$ meV. The line was obtained by fitting the I_c spectrum in the 1.4585–1.4781 eV range. It coincides with I_c within a noise of $\sim 1\%$ of the peak value up to 1.479 eV. Above this value the difference from the measured signal resembles a broadened steplike onset of the continuum, with a superposed lh exciton band at ~ 1.503 eV.

According to Eq. (5) the I_c and ε_2 profiles differ due to the dispersion of the refractive index n , the spectral dependences of the self-absorption term $1/(\alpha_x + \alpha)$, and the probability of transmission at the sample surface $(1-R)$. In order to justify the use of the LG profiles (derived for ε_2) for the low-energy tail of I_c , we have to estimate the influence of the three factors. The refractive index is high due to the strong interband absorption in the ultraviolet (uv) region (above ~ 3 eV). For example, for the 83.8-Å MQW sample we have found $n(E) \approx 3.046 + 0.165E^2$ (with E in eV) from the interference of the normal-incidence reflectance in the 1.25–1.45 eV region at room temperature. The quadratic term accounts for dispersion due to uv absorption. Its extrapolation to the narrow range of the hh- e excitons gives a negligible change of n : the increase across the 1.46–1.48 eV range of the broadest band above room temperature (see Fig. 6) is 0.0097. There is also a spectral change of n due to the exciton absorption band itself. Namely, we have to add the real part of the ε_{LG} of Eq. (10) to the background dielectric function $\varepsilon_1 = n^2(E) \approx 9.28 + 1.01E^2$. The curves of Fig. 2 show that this contribution does not exceed $\sim 60\%$ of the height of the peak in ε_2 , and its variation on the low-energy wing is even smaller. We can estimate the peak value of ε_2 using the linear

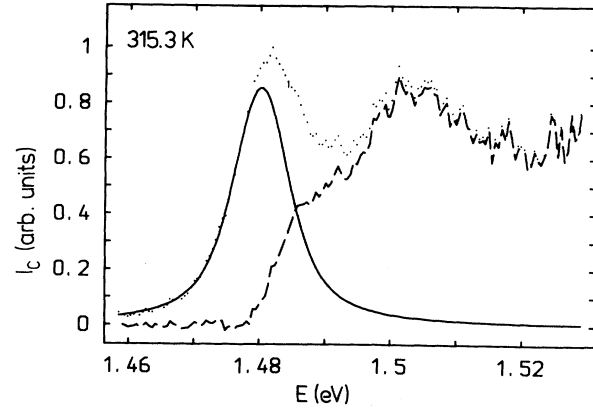


FIG. 6. Measured I_c spectrum of the 83.8-Å MQW at 315.3 K (dots). The LG profile fitted to the low-energy wing of the experimental data is indicated by the solid line, the difference by the broken line.

expansion of the reflectivity.¹⁰ The derivatives of R with respect to ε_1 and ε_2 exhibit interference patterns due to the multiple reflections in the MQW film with the maximum values of $|dR/d\varepsilon_1| \approx |dR/d\varepsilon_2| \approx 0.06$ in our spectral range. Since the height of the exciton peak seen in the reflectivity of Fig. 3 is about 0.03, the peak value of ε_2 is ≤ 0.5 . The corresponding contribution to $\varepsilon_1 \approx 12$ just below the exciton peak is, therefore, less than ~ 0.3 ; this leads to a fairly small maximum increase of the refractive index, $\sqrt{12.3} - \sqrt{12} \approx 0.04$, expected across the fitted part of the I_c profile. The spectral dependence of the transmission factor $(1-R)$ in Eq. (5) is also weak and acts in the opposite direction, i.e., it reduces I_c going from lower energies towards the exciton peak.

The flat spectral shape of $n(1-R)$ is, of course, due to the high polarizability related to uv absorption, which leads to the high background ε_1 and only to a small modification due to excitonic bands. On the other hand, neglecting the self-absorption term $1/(\alpha_x + \alpha)$ relies on the assumption of $\alpha_x \gg \alpha(E)$. The estimate of $\varepsilon_2 \leq 0.5$ for the hh exciton peak implies $\alpha \leq 1.1 \times 10^4$ cm⁻¹ at $E = 1.5$ eV. The absorption coefficient measured ellipsometrically⁹ at the exciting photon energy $E_x = 1.96$ eV is $\alpha_x \approx 3 \times 10^4$ cm⁻¹ for both of our samples. With the cutoff energy at $\sim 75\%$ of the peak height, the absorption coefficient in the fitted region reaches up to $\sim 25\%$ of α_x ; this means that $1/(\alpha_x + \alpha)$ falls to $\approx 80\%$ of its limiting value of $1/\alpha_x$ that is reached rapidly with decreasing photon energy. Returning to the data of Fig. 4 we could speculate that the displayed discrepancy of the measured and model line shapes in the broader range was, at least in part, due to the neglected self-absorption factor $1/(\alpha_x + \alpha)$. If this were the only reason, however, the energy E_0 would not be shifted to higher values as shown in Fig. 5. The onset of the higher-lying absorption mentioned above is needed to explain the observed behavior. We conclude that, although it is the most serious reason for some differences between the I_c and ε_2 line shapes, we can neglect the influence of self-absorption in our spectra.

Let us note that it becomes much more important when the exciting light of power energies is used.

V. DISCUSSION

The temperature dependence of the hh exciton energy E_0 obtained for the 78.1-Å MQW sample from fitting the low-energy tail of I_c by the LG profiles is shown in Fig. 7. This dependence follows closely the empirical relation for the lowest direct band gap of bulk GaAs,¹⁴ $E_{\text{GaAs}}(T) = 1.519 - 0.0005408T^2/(T+204)$, shifted rigidly by $\Delta = 71.5 \pm 1.0$ meV towards higher energies. The shift Δ represents the sum of the electron and heavy-hole localization energies and of the binding energy of the hh-e exciton. For the 83.8-Å MQW the value $\Delta = 66.5 \pm 1.0$ meV was obtained. For both samples a significant deviation of the PL peak position from both E_0 and $E_{\text{GaAs}} + \Delta$ is observed at the lowest temperatures. This is essentially due to the strong influence of the Boltzmann factor of Eq. (5) that suppresses the luminescence at the exciton energy E_0 and prefers the emission of low-energy photons. The minor systematic difference between E_0 and $E_{\text{GaAs}} + \Delta$ at the lowest temperatures is probably due to the limitations of the empirical Varshni formula used to model the temperature dependence of E_{GaAs} . The good agreement of the energies E_0 with the shifted direct energy gap of GaAs confirms that the parameter values obtained from fitting the low-energy wing of I_c are representative of the whole profiles, including their centers. The inset of Fig. 7 shows the shift of the PL peak position from E_0 on expanded scales. The experimental points follow closely the dependence predicted by computing numerically the peak positions for the corresponding LG profile with temperature-independent Γ_L and Γ_G . In the computation, we have used the values of 0.4 and 2.8 meV, respectively; these are the mean values obtained from the fitting of the whole series of the I_c spectra at the lowest temperatures. Since $\Gamma_L \ll \Gamma_G$, the actual temperature depen-

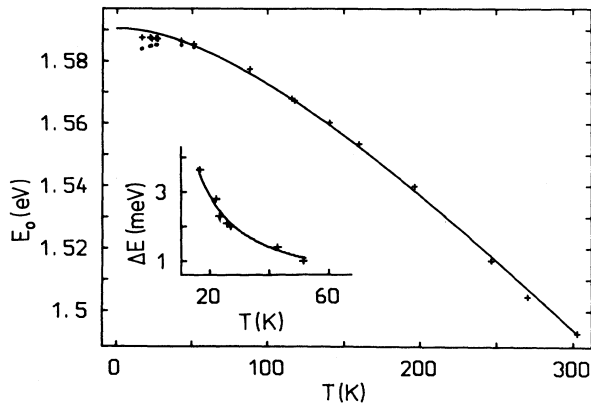


FIG. 7. Exciton energies E_0 obtained for the 78.1-Å MQW by fitting the low-energy tails of I_c (crosses), peak positions E_p of the PL signal I (solid circles), and direct energy gap of bulk GaAs shifted upwards by 0.0715 eV (solid line). The inset shows the difference $E_0 - E_p$ as observed (crosses) and computed for the LG profile with $\Gamma_L = 0.4$ meV, $\Gamma_G = 2.8$ meV (solid line).

dence of Γ_L , shown in Fig. 8 and discussed below, does not change significantly the computed ΔE . The random deviations of the experimental points from the smooth computed line in the inset of Fig. 7 are, of course, due to the scatter of both peak positions and best-fit parameters for the individual spectra.

Thus, the asymmetry of the PL line, accompanied by the Stokes shift of its peak position, is accounted for by the assumption of the detailed thermodynamical balance. The tendency for intrinsic free-exciton emission of high-quality GaAs quantum wells is in sharp contrast to the usual extrinsic (defect-related) nature in the comparable bulk material, see, e.g., Ref. 2 and references therein.

The broadening energies Γ_L and Γ_G were obtained from the fitting of the I_c line shapes in two stages. First, both of them were fitted simultaneously with the two remaining parameters (F and E_0) of the LG profile. The profiles are nearly Gaussian at low temperatures: $\Gamma_G = 3.2 \pm 0.1$ meV, $\Gamma_L = 0.4 \pm 0.3$ meV, and $\Gamma_G = 2.8 \pm 0.1$ meV; $\Gamma_L = 0.3 \pm 0.3$ meV was the result at 16 K for the 83.8- and 78.1-Å MQW samples, respectively. With increasing temperature, the Gaussian width remains constant within the error limits, while Γ_L increases. Thus, the inhomogeneous broadening (i.e., that due to structural imperfections of the samples) leads to the Gaussian profile of I_c . The degradation of the signal-to-noise ratio with increasing temperature causes a rather steep increase of the errors, as shown for Γ_G in Fig. 8. We have therefore fixed Γ_G at its low-temperature mean value and fitted the three remaining parameters in the second stage. This reduces the scatter of the retrieved Γ_L to a few tenths of meV even at room temperature. The Lorentzian parameters plotted in Fig. 8 were obtained in this way.

The observed increase of Γ_L with temperature is somewhat flatter than that predicted by the scattering of excitons by absorbing longitudinal-optic (LO) phonons of the energy $\hbar\omega_{\text{LO}} \approx 36$ meV in GaAs. Using a single temperature-independent parameter γ in describing the

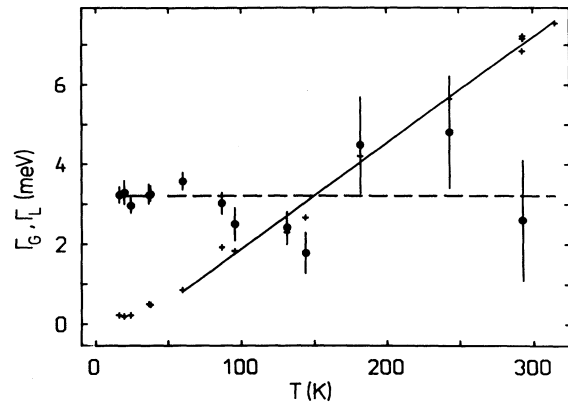


FIG. 8. Lorentz (crosses; obtained with Γ_G fixed at 3.2 meV) and Gauss (solid circles with error bars; obtained with both Γ_L and Γ_G fitted simultaneously) broadening energies for the 83.8-Å MQW sample. The mean value of Γ_G below 50 K is indicated by the horizontal dashed line. The solid line is the best-fit linear dependence of Γ_L above 50 K.

TABLE I. Parameters of the studied GaAs/AlAs MQW samples; γ is the temperature-independent measure of the strength of scattering by LO phonons defined by Eq. (13).

Sample	A	B
Well width (Å)	83.8±0.5	78.1±0.5
Monolayers	29.6	27.6
$E_0 - E_{\text{GaAs}}$ (meV)	66.5±1.0	71.5±1.0
Γ_G (meV)	3.2±0.1	2.8±0.1
Γ_L (meV), $60 \leq T \leq 320$ K	0.79 + 0.0265(T - 60)	0.68 + 0.0296(T - 60)
γ (meV), $250 \leq T \leq 320$ K	11±1	12±1

strength of the exciton-LO-phonon scattering via⁵

$$\Gamma_L/2 = \gamma / [\exp(\hbar\omega_{\text{LO}}/kT) - 1] \quad (13)$$

for the temperatures above ~ 250 K, we have obtained the results listed in Table I. The strength is doubled compared with the value of 5.5 meV found for a MQW structure with 102-Å GaAs wells and $\text{Al}_{0.28}\text{Ga}_{0.72}\text{As}$ barriers⁵ and seems to increase with decreasing well width. Our values of γ are also higher than 9.26 meV found for a 53-Å GaAs MQW structure with $\text{Al}_{0.27}\text{Ga}_{0.73}\text{As}$ barriers.⁷ In our opinion, the simple evaluations of the full or half width of the excitonic structure are unreliable, especially for the strongly asymmetric line shapes at higher temperatures. The overlap with higher-energy structures and uncertain base lines makes the task of determining the width rather difficult. The extrapolation of Eq. (13) towards lower temperatures gives much lower values of Γ_L than observed experimentally (e.g., $\Gamma_L \approx 0.34$ - and 0.38-meV result at $T=100$ K for the 83.8- and 78.1-Å MQW, respectively while the actual Lorentzian width is ~ 1.9 meV for both samples). This indicates an important contribution of other scattering processes for the homogeneous linewidth. Let us note that our values of Γ_L at the lower end of the linear range are comparable with the widths reported for GaAs *single* QW samples. Namely, we observe $\Gamma_L = 0.8 \pm 0.2$ and 0.7 ± 0.2 meV at 60 K for the two samples of Table I, respectively; the FWHM of 0.75 ± 0.02 and 1.00 ± 0.04 meV were observed at this temperature for single QW samples with a small inhomogeneous broadening for the well widths of 135 and 277 Å.¹⁵

Of course, our samples are not suitable for a study of the homogeneous width at the lowest temperatures, because of the dominating inhomogeneous broadening. The slightly lower value of the inhomogeneous width in the 78.1-Å sample results from the fact that the interface quality and the homogeneity of the wells and barriers was incidentally better than in the 83.8-Å sample. The PL linewidths and positions were remarkably constant over the area of about 1×1 cm² for both samples. Let us note that we have observed the expected increase of the linewidths in other structures with thinner QW's; this was typically accompanied by pronounced fluctuations of their positions across the sample surfaces. The difference of 5.7 Å in the mean well thickness of both samples corresponds to ~ 2.0 monolayers (ML's) of GaAs. Consequently, the observed difference of 5.0 meV of the exciton energy implies a rough estimate of 2.5 meV/mL for the

energy shift per monolayer near the mean well width of 81 Å. The inhomogeneous Gaussian widths of Table I are compatible with the standard deviations of the mean thickness only slightly higher than 1 ML, both across the sample surface and along the growth direction. In other words, the disorder at the interfaces is confined essentially to a border single monolayer in all QW's in the MQW structure. This degree of structural perfection obtained with the MBE growth technique is a substantial factor in achieving the easily detectable PL signals even above room temperature.

VI. CONCLUSIONS

Detailed studies of the PL line shapes of two well-characterized GaAs/AlAs MQW structures have led to a complete understanding of the lowest hh-*e* excitonic line profile in the wide temperature range from 16 to 320 K. A correction of the PL signal based on the assumption of the detailed thermodynamical balance in the exciton system leads to line shapes proportional to absorption profiles. The influence of self-absorption and dispersion of the refractive index was found to be negligible. The line shapes are easy to interpret since they are free from interference effects of multiple reflections within MQW films. A suitably chosen portion of the low-energy tail of the hh exciton line does not overlap with higher excitations; however, it still contains enough information concerning the position and broadening of the line. These spectra are fitted excellently with Lorentz-Gauss profiles that can be computed efficiently using the complex probability function. The inhomogeneous broadening is found to have a Gaussian shape, with spectral widths corresponding to the standard deviations of about one monolayer of QW thickness. The Lorentzian component increases nearly linearly with temperature in the range from 50 to 320 K. The strength of the LO-phonon scattering derived from its room temperature value is about twice as high as reported previously for GaAs/ $\text{Al}_x\text{Ga}_{1-x}\text{As}$ MQW structures. The hh exciton energy follows closely the direct gap of GaAs, shifted by a constant value throughout the whole temperature interval. The asymmetry of the PL line, accompanied by the Stokes shift of its peak position observable in the 16–60 K region in our MQW structures, is accounted for quantitatively by the line-shape analysis. The origin of the

Stokes shift is different from the usual defect-related lowering of the emission energy with respect to the corresponding absorption line. It is observed for quantum wells of very high structural homogeneity, where it is not masked by the geometrical effects of fluctuating well widths.

ACKNOWLEDGMENTS

We would like to thank M. Cardona for useful discussions and critical reading of the manuscript. The expert help of A. Fischer with the MBE growth is gratefully acknowledged.

-
- ¹S. Schmitt-Rink, D. S. Chemla, and D. A. B. Miller, *Adv. Phys.* **38**, 89 (1989).
- ²R. C. Miller and D. A. Kleinman, *J. Lumin.* **30**, 520 (1985).
- ³R. C. Miller, D. A. Kleinman, W. A. Nordland, Jr., and A. C. Gossard, *Phys. Rev. B* **22**, 863 (1980).
- ⁴C. Weisbuch, R. C. Miller, R. Dingle, A. C. Gossard, and W. Wiegmann, *Solid State Commun.* **37**, 219 (1981).
- ⁵K. J. Nash and D. J. Mowbray, *J. Lumin.* **44**, 315 (1989).
- ⁶T. Takagahara, *J. Lumin.* **44**, 347 (1989).
- ⁷S. Selci, A. Cricenti, M. Righini, C. Petrillo, F. Sacchetti, F. Alexandre, and G. Chiarotti, *Solid State Commun.* **79**, 561 (1991).
- ⁸J. Humlíček, F. Lukeš, and K. Ploog, *Phys. Rev. B* **42**, 2932 (1990).
- ⁹J. Humlíček, F. Lukeš, K. Navrátil, M. Garriga, and K. Ploog, *Appl. Phys. A* **49**, 407 (1989).
- ¹⁰J. Humlíček, F. Lukeš, and K. Ploog, *Superlatt. Microstruct.* **9**, 133 (1991).
- ¹¹W. van Roosbroeck and W. Shockley, *Phys. Rev.* **94**, 1558 (1954).
- ¹²V. N. Faddeyeva and N. M. Terent'ev, *Tables of Values of the Function $w(z)$ for Complex Argument* (Pergamon, Oxford, 1961).
- ¹³J. Humlíček, *Analysis of Spectrum Line Profiles*, *Folia Fac. Sci. Nat. Univ. Brunensis Tomus XXV, Physica* **36** (1984).
- ¹⁴*Numerical Data and Functional Relationships in Science and Technology*, edited by O. Madelung and M. Schulz, *Landolt-Börnstein, New Series, Group III, Vol. 22, Pt. a* (Springer, Berlin, 1987), p. 82.
- ¹⁵L. Schultheis, A. Honold, J. Kuhl, K. Koehler, and C. W. Tu, *Phys. Rev. B* **34**, 9027 (1986).